Hydrogen spillover enabled active Cu sites for methanol synthesis from CO_2 hydrogenation over Pd doped CuZn catalysts

Bing Hu[a], Yazhi Yin[a], Guoliang Liu[a]*, Shengli Chen[a], Xinlin Hong[a]* and Shik Chi Edman Tsang[b]

[a] *College of Chemistry and Molecular Sciences, Wuhan University, Wuhan 430072, PR China.* [b] *Wolfson Catalysis Centre, Department of Chemistry, University of Oxford, Oxford, OX1 3QR, UK.*

* Corresponding authors:

Email address: hongxl@whu.edu.cn; liugl@whu.edu.cn;

Abstract

Surface modification with Pd is an effective way for improved activity in CO_2 hydrogenation to methanol over commercial Cu-ZnO catalysts *via* a so-called hydrogen spillover mechanism. However, there still lacks a quantitative analysis of hydrogen spillover effect and the nature of active sites after Pd modification remains unclear. In this work, we prepared a series of Pd-doped Cu-ZnO catalysts (Pd-CZ-x) with tunable Pd loading by using a facile polyol reduction method for a deep study of the promotion effect of Pd. With the increase of Pd/Cu molar ratio (x) from 0 to 0.04, there emerges a volcano-shaped relationship between methanol space time yield (STY) and Pd loading. 1% Pd doping can increase the methanol STY by 2.5 times and the methanol turnover frequency (TOF) by 3.5 times at 543 K, when compared to undoped Cu-ZnO. Kinetic studies show the activation energy required for methanol synthesis is greatly reduced from 59 kJ mol^{-1} over Cu-ZnO to 31 kJ mol^{-1} over Pd-CZ-0.01. Behind the volcano-shaped relationship is a balance between the hydrogen spillover effect of Pd and the reduced surface Cu area caused by Pd blocking. Chemisorption gives a quantitative analysis of the reducible Cu sites ($Cu_{red.}$) enabled by hydrogen spillover. Importantly, it is found that the methanol STY correlates linearly with $Cu_{red.}$ surface area, suggesting that the activated Cu sites enabled by hydrogen spillover are real active sites for methanol synthesis from CO_2 hydrogenation.

Key words: CO_2 hydrogenation; hydrogen spillover; Pd doped CuZn catalysts; reducible Cu; active sites

1. Introduction

Catalytic methanol synthesis from CO_2 is one of the most important reactions in industry because methanol is a platform chemical for the manufacture of fuels and value-added chemicals [1-6]. Cu-ZnO based catalysts, commercially used for methanol synthesis from syngas, are also active for CO_2 hydrogenation to methanol [7-9]. However, they still suffer from low methanol yield and considerable activity for CO formation *via* the reverse water gas shift (RWGS) reaction ($CO_2 + H_2 \rightarrow CO + H_2O$) [10,11]. Hence, the conventional CuZn catalysts have been widely modified with different metal oxides as a support such as ZrO_2, Ga_2O_3, CeO_2, MgO and Cr_2O_3, etc [12-16]. These supports were believed to modulate the basicity to enhance adsorption of CO_2 and related C1 intermediate species [17-19], to improve the dispersion of surface Cu^0 moiety [13,14] or to prevent the catalyst from deactivation by water vapor [20], etc.

Another strategy is to improve the capability of hydrogen dissociation over CuZn catalysts by adopting a promoter to increase the hydrogen activation [21,22]. Pd has been found to be efficient in improving methanol formation over Cu-ZnO catalyst. Melian-Cabrera et al. reported Pd as a good promoter for methanol synthesis with improved activity by maintaining the reduced state of Cu via hydrogen spillover [23-25]. Sahibzada et al. further confirmed the promotion effect of hydrogen spillover on both methanol selectivity and yield by physically mixing Pd-Al_2O_3 with the Cu-ZnO catalyst [26]. Although the hydrogen spillover was evidenced between Pd and Cu sites to enhance the reaction rate, the nature of active sites still remains unclear. Moreover, PdCu and PdZn bimetallic phases have also been reported as active sites for methanol synthesis [27,28]. The complexity of surface sites (Pd, Cu, PdCu, PdZn, CuZn, et. al.) would make it rather difficult to identify the real active sites in the Pd modified CuZn catalysts.

To address above issues, it is very important to prepare ternary Pd-Cu-Zn catalysts with as well-defined surface sites as possible. The variation in Pd incorporation

methods (i.e., co-precipitation versus sequential precipitation) was reported to have the opposite effect on the catalytic performance in the hydrogenation of CO_2 to methanol [25]. Polyol has been widely used to reduce metal cations into metal nanoparticles in nanoparticle synthesis [29-31]. Besides, the polyol system was successfully used to prepare ZnO aggregates with a high surface area [32]. Such progress inspired us to synthesize Pd-Cu-ZnO complex by using a one-pot polyol method. Here, the aim of this work was to explore the promotion effect of Pd on CuZn catalysts and to identify the nature of active sites for methanol synthesis after Pd modification. A series of Pd-doped Cu-ZnO catalysts with tunable Pd loading was facilely prepared using a polyol reduction method in diethyl glycol. A proper amount of Pd doping was confirmed to improve the catalytic performance through the hydrogen spillover effect which created more reducible surface Cu sites as active sites for CO_2 hydrogenation to methanol.

2. Experimental

2.1 Catalyst preparation

The Cu/Zn molar ratio in the series of Cu-based catalysts was fixed at 1:1 so as to explore the effect of Pd modification to the system.

The Cu-ZnO catalyst was synthesized in the following procedure. 1.9965 g of $Cu(CH_3COO)_2 \cdot H_2O$ (10 mmol, ≥98% pure, Sinopharm Chemical Reagent) and 2.1951 g of $Zn(CH_3COO)_2 \cdot 2H_2O$ (10 mmol, ≥99% pure, Sinopharm Chemical Reagent) were dissolved in 100 mL of diethylene glycol (DEG, ≥99% pure, Sinopharm Chemical Reagent) in a three-neck round-bottom flask with the help of vigorous magnetic stirring and ultrasonication. The flask was then transferred into an oil bath to heat the solution rapidly to reflux at around 462 K under vigorous stirring and under the protection of N_2 flow. The reaction was maintained for 8 h and then cooled down naturally. The precipitates were collected by centrifugation and washed with distilled water and ethanol each by 3 times, followed by a vacuum drying at 333 K for 12 h. The product is denoted as CZ.

Pd-doped Cu-ZnO catalysts were synthesized in a similar procedure with the only difference being the co-addition of Na_2PdCl_4 (≥98% pure, Aladdin), from 0.0147 to 0.1176 g, with the Cu and Zn precursors in the initial step. The Pd/Cu molar ratio was varied from 0.005 to 0.01, 0.02, 0.03 and 0.04. The final product was denoted as Pd-CZ-x, where x stands for the molar ratio of Pd to Cu in the initial recipe.

2.2 Characterization

Unless noted otherwise, before each characterization, the as-synthesized catalyst was reduced under H_2 flow, cooled down under Ar followed by swift transfer into small glass vessel with a perforated rubber cap and then into a Schlenk tube deoxygenated by Fe powder and then vacuumed and refilled with N_2.

Transmission Electron Microscopy (TEM) images were acquired on a JEM-2100 (JEOL) to observe the morphology of the catalysts. Elemental mapping was performed on a Technai G2 F20 (FEI) equipped with scanning TEM (STEM) accessories. N_2 sorption measurements were conducted at 77 K on a ASAP 2020 (Micromeritics) and the Brunauer-Emmett-Teller (BET) multilayer-sorption model was used to calculate the surface area while the Barrett-Joyner-Halenda (BJH) method was used for pore volume calculation. Inductively coupled plasma-atomic emission spectroscopy (ICP-AES) analysis was performed on an IRIS Intrepid II XSP equipment (Thermo) to measure the active metal content in the as-synthesized catalysts. Powder X-ray diffraction (XRD) patterns of the reduced catalysts were recorded on a Bruker D8 Advance with Cu Kα radiation. Powder Diffraction Files, #04-0836 (Cu) and #36-1451 (ZnO), are used to recognize the crystallite phase. Scherrer equation was used to calculate the crystallite sizes.

X-ray photoelectron spectroscopy (XPS) measurements were carried out in a custom made device (Scienta Omicron) equipped with a gas-reaction chamber. The sample was pressed into a tablet and then placed in the pretreatment chamber to be reduced under 20 mL min^{-1} H_2 at 573 K (heating rate: 5 K min^{-1}) for 2 h. After it is cooled down, the tablet was transferred into the test chamber to measure the XPS

spectra for the reduced catalyst. No adventitious carbon is used as internal standard during XPS test with regard to the inevitable carbon residue on the catalysts surface in polyol reduction method. The C-C component of C1s was fitted out and calibrated to 284.8 eV, which provided the binding energy (BE) calibration for elements in the same set of measurement.

H_2 temperature-programmed desorption (H_2-TPD) experiments were carried out on a BEL-CAT B (BEL, Co., Japan) to examine the hydrogen adsorption properties of the catalysts. In each test, 0.1 g of sample was loaded into the quartz tube and was reduced in a flow of 5% H_2/Ar (30 mL min^{-1} at 573 K (heating rate: 5 K min^{-1}) for 2 h and cooled down to 303 K in 30 mL min^{-1} of 5% H_2/Ar. Then Ar flow (30 mL min^{-1}) was used to purge the residual H_2 for 1h. After the above pretreatment was done, the carrier gas was switched to Ar at a flow rate of 10 mL/min and the temperature was elevated to 1123 K at a rate of 10 K min^{-1} while the TCD recording was concurrently started.

Temperature-programmed reduction (TPR) experiments were performed on a BEL-CAT B (BEL, Co., Japan) in order to study the surface copper species in the catalysts. 0.1 g of sample was used in each individual test. The pretreatment steps were as follows. First, the catalyst was reduced under 5% H_2/Ar flow (30 mL min^{-1}) at 573 K (heating rate: 5 K min^{-1}) for 2 h and cooled down to 313 K under Ar flow (20 mL min^{-1}). Then N_2O was passed through (20 mL min^{-1}) the sample to oxidize the surface species at 333K for 1h. And then the sample temperature was raised to 423 K (heating rate: 5 K min^{-1}) under Ar flow at a rate of 20 mL min^{-1} and hold at 423 K for 30 min to purge residual N_2O. Finally, the sample temperature was cooled down to 313 K. After the pretreatment is done, the gas was switched to 5% H_2/Ar (30 mL min^{-1}) and the sample temperature was ramped to 553 K at a rate of 10 K min^{-1} and thermal conductivity detector (TCD) recording was started to obtain surface-H_2-TPR profile. TPR peak area was integrated and transformed into H_2-consumption based on calibration. The number of surface copper atoms is twice the number of H_2 molecules

consumed as shown in Eq. (1) and Eq. (2).

$$2Cu\ (surface) + N_2O \rightarrow N_2 + Cu_2O \quad (1)$$

$$Cu_2O + H_2 \rightarrow 2Cu + H_2O \quad (2)$$

2.3 Catalytic test

A continuous-flow, tubular fix-bed reactor was used to evaluate the catalytic activity. 0.2 g of catalyst was loaded into the stainless steel tube filled with an appropriate amount of quartz fiber. Before catalytic test, the catalyst was reduced in 20 mL min^{-1} of H_2 at 573 K (heating rate: 5 K min^{-1}) for 2 h. After cooling down to 423 K, a CO_2/H_2 mixture with a molar ratio of 1:3 was fed at a rate of 400 mL min^{-1} to reach 4.5 MPa set by the back pressure valve. Then the flow rate was adjusted to 36 mL min^{-1} (corresponding to a gas hourly space velocity (GHSV) of 10800) and the temperature was elevated at 5 K min^{-1} to the desired reaction temperature within the range of 503 K-543 K. Post-reactor lines and valves were heated up to 423 K to avoid products condensation. The products were analyzed online by a gas chromatography (GC) equipped with a TCD detector and Porapak-Q column. Conversion and selectivity were calculated from the last three sets of GC spectra collected every 5 min throughout a reaction time of 3 h.

3. Results and discussion

3.1 Materials characterization

The Cu-ZnO and Pd-doped Cu-ZnO catalysts were prepared using a one-pot polyol reduction method, denoted as CZ and Pd-CZ-x respectively, where x represents the molar ratio of Pd to Cu. The morphology and microstructures were first examined by using transmission electron microscopy (TEM). As shown in Fig. 1a and Fig. S1, all samples show blackberry-shaped microstructures of up to 200 nm, with each “berry” composed of numerous nanospheres of about 20 nm in the average size. Fig. 1b shows high resolution TEM images of the typical Pd-CZ-0.01 sample. Clearly, the lattice fringes of bimetallic CuPd (111), (200) and Pd (111) in the vicinity of ZnO (100), provide evidence for the high dispersion of Pd, mainly in form of CuPd alloy phase

within the catalyst. The elemental mapping was then acquired by using high-angle annular dark-field STEM (HAADF-STEM) with energy dispersive X-ray spectrometer (EDX), explicitly showing a homogeneous distribution of O, Zn, Cu and Pd through the entire framework within a berry (Fig.s 1c and d). Similar profiles for the Pd-CZ-0.03 and Pd-CZ-0.04 samples were also demonstrated (Fig. S2).

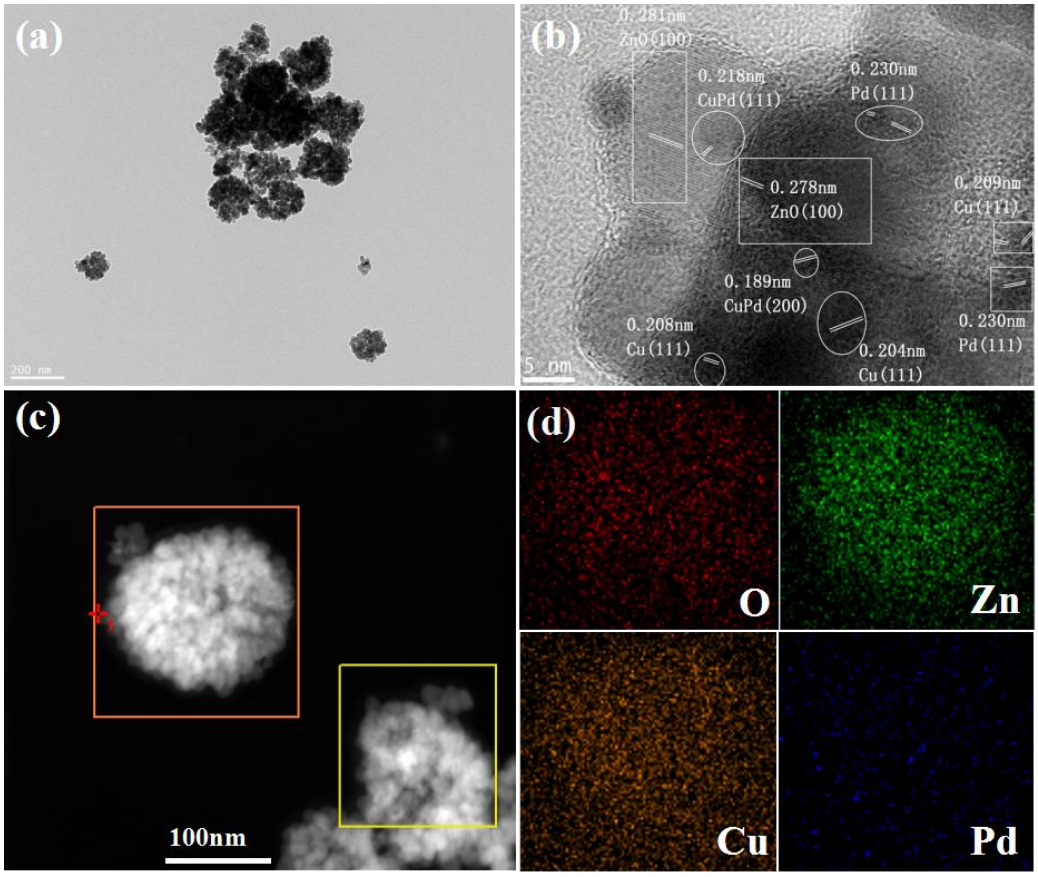

Fig. 1 (a) TEM, (b) HR-TEM and (c) HAADF-STEM images of the typical Pd-CZ-0.01 sample and the corresponding (d) elemental mapping from (c). In (c), the orange rectangle is the area for elemental mapping and the yellow rectangle serves for drift correction.

X-ray photoelectron spectra (XPS) were then performed to probe the chemical state of Cu, Zn and Pd for the CZ and Pd-CZ-x catalysts, as illustrated in Fig. S3. All samples show identical binding energies (BE) of Zn 2*p* and Cu 2*p*, suggesting the same oxidation state of Zn and Cu before and after the doping of Pd. Combining with the modified Auger parameters [33] (AP, defined as AP = BE ($2p_{3/2}$) - BE ($_{LMM}$) +

X-ray energy) of Zn (1850.65-1850.82 eV) and Cu (2009.50-2009.61 eV) (Table S1), we confirmed the chemical state of Zn^{2+} and Cu^0 in all catalysts with reference to Wagner Plot [34]. XPS spectra of Pd 3*d* for all Pd-CZ-x samples show two peaks at 335.4 and 340.7 eV, which can be assigned to the $3d_{5/2}$ and $3d_{3/2}$ of Pd^0. Note that the reported binding energies of Pd^0 in PdCu alloy and metallic Pd are very close, making them difficult to be differentiated from Pd 3*d* core-level spectra [27]. However, we could still rule out the presence of PdZn from our Pd-CZ-x samples because PdZn alloy phase shows a more positive BE than metallic Pd [35].

Fig. 2a shows the powder X-ray diffraction (XRD) patterns of the reduced CZ and Pd-CZ-x catalysts. All samples exhibit a series of typical diffraction peaks (labelled as circle) indexed to wurtzite ZnO (JCPDS#36-1451) while the diffraction peaks at 43°, 51° and 74° (labelled as inverted triangle) are assigned to metallic Cu (JCPDS#04-0836). No recognizable Pd diffractions appear in the patterns of the Pd-CZ-x samples due to the low Pd loading and good dispersion. Notably, the Cu diffractions are much sharper than the ZnO peaks, indicating a larger crystalline size of Cu than that of ZnO. Table S2 displays the average particle size of Cu and ZnO as calculated from Scherrer formula. It can be seen the Cu particle size generally decreases from 37.9 to 22.0 nm with the increase of Pd/Cu molar ratios from 0 to 0.04 while the ZnO particle size remains unperturbed (16.4±0.7 nm) This somehow indicates that Pd can modulate the formation of Cu particles rather than ZnO crystals. Moreover, in Fig. 2b the Cu (111) peak gradually shifts towards low angle with the increase of Pd loading, suggesting a lattice expansion of Cu due to a larger atomic radius of Pd than Cu. This can further support the successful doping of Pd into the Cu lattice.

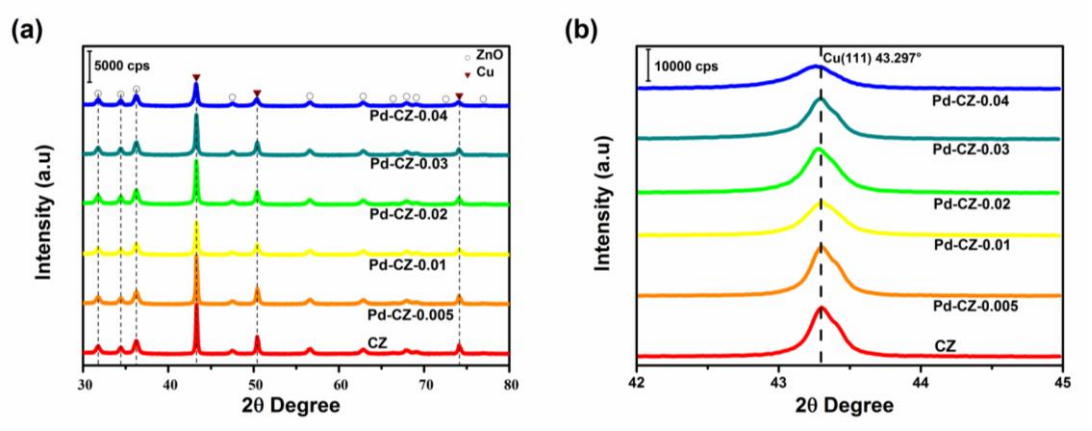

Fig. 2 The XRD patterns of the CZ and Pd-CZ-x catalysts. (a) The wide-range patterns show the typical diffraction peaks indexed to wurtzite ZnO and metallic Cu. (b) The magnified Cu (111) peak displays a gradual shift towards low angle with increased Pd loading, suggesting a lattice expansion of Cu.

Fig. S4 displays the nitrogen sorption isotherms of all samples, where a type IV isotherm with a type H3 hysteresis loop is observed, indicative of abundant mesopores formed by the stacking of particles in the materials [36]. All samples possess very similar Brunauer-Emmett-Teller (BET) surface area of about 20 m^2 g^{-1} (Table S3). The contents of Cu and Pd were detected by ICP-OES and listed in Table S3. The Pd contents for all Pd-CZ-x samples were slightly lower than the theoretical values (calculated from recipe) while the Cu contents were opposite, which may be explained by the different reduction potentials of Cu and Pd.

3.2 Catalytic performance

We next evaluated the CZ and Pd-CZ-x catalysts in the hydrogenation of CO_2 to methanol at different temperatures from 503 to 563 K. Fig. 3 and Table S4 show the catalytic results including the conversion of CO_2, the selectivity to methanol, and the space time yield (STY) of methanol and CO. Note that CO is generated as the exclusive carbonaceous byproduct via the reversed water gas shift (RWGS) reaction. The RWGS reaction is endothermic, with an enthalpy change of 41.2 kJ mol^{-1} at 298 K, whilst the title reaction (CO_2 hydrogenation to methanol) is exothermic (-49.5 kJ mol^{-1}) [37], as seen in Equations 3 and 4. Thermodynamically, the selectivity to methanol will drop as the reaction temperature increases, in good agreement with the

decreasing trend of methanol selectivity for all samples (Fig. 3a). The methanol selectivity declines sharply from 62% at 503 K to 41% at 563 K for the CZ catalyst, but it only drops from 73% to 69% for the Pd-CZ-0.04 sample. This suggests that the doping of Pd favors a narrow variation range of methanol selectivity with reaction temperature. Also the doping of Pd could improve the methanol selectivity to some extent, which is distinctive at a high reaction temperature. Importantly, the methanol selectivity of Pd-CZ-0.01 reaches 73% at 523 K, which is much higher than that of the CZ sample (59%) in this work and previously reported Cu-based catalysts (below 55% under approximate reaction condition) [38,39], and comparable to that of advanced Pd/ZnO catalysts (70-80%) [4]. So, Pd doping is indeed an effective way to increase the methanol selectivity of commercial CuZn catalysts.

$$CO_2 + 3H_2 \rightarrow CH_3OH + H_2O \qquad \Delta H_{298\,K} = -49.5\ kJ\cdot mol^{-1} \qquad (3)$$

$$CO_2 + H_2 \rightarrow CO + H_2O \qquad \Delta H_{298\,K} = 41.2\ kJ\cdot mol^{-1} \qquad (4)$$

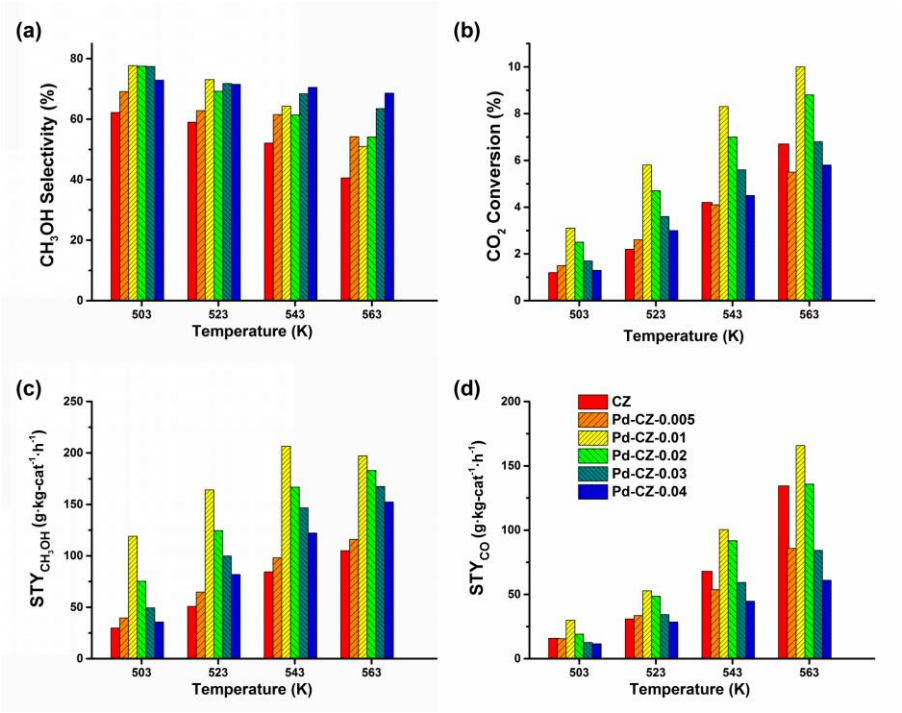

Fig. 3 (a) Methanol selectivity, (b) CO_2 conversion, (c) methanol STY and (d) CO STY in methanol synthesis from CO_2 hydrogenation over a series of catalysts. Reaction conditions: 4.5

MPa, H_2/CO_2 = 3 and GHSV = 10800.

Regarding the CO_2 conversion, it shows an increasing trend with reaction temperature for all the catalysts, suggesting that high temperatures would favor the activation of CO_2. Precisely, the CO_2 conversion over the CZ sample increases by nearly 6 times from 1.2% to 6.7% when the temperature was raised from 503 to 563 K. In contrast, the CO_2 conversion over the Pd-CZ-0.01 samples is only enhanced by about 3 times from 3.1% to 10.0%, which is less sensitive to the reaction temperature than that over the CZ sample. This indicates the activation energy (E_a) required for CO_2 hydrogenation decreases after the 1% doping of Pd. It is also found that the Pd-CZ-0.01 catalyst shows the highest CO_2 conversion among the six samples in the temperature region from 503 to 563 K.

As for the methanol yield, we can see a volcanic correlation of STY versus the loading of Pd at all tested temperatures, with the Pd-CZ-0.01 catalyst showing the best performance (Fig. 3c). Notably, the methanol STY over the Pd-CZ-0.01 catalyst reaches the highest value (207 g kg_{cat}^{-1} h^{-1}) at 543 K, 2.5 times that of the undoped CZ catalyst (84 g kg_{cat}^{-1} h^{-1}). The sudden drop of the methanol STY at a higher temperature (563 K) may result from the limitation of thermodynamic equilibrium state [40]. The STY of the byproduct CO was also correlated with the Pd loading, and a very similar volcanic profile was observed, irrespective of the high STY over the CZ sample at 543 and 563 K (Fig. 3d).

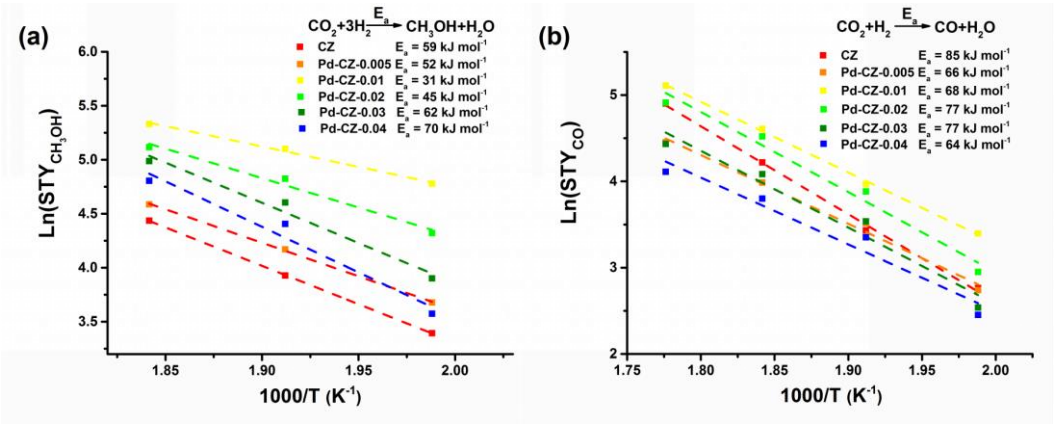

Fig. 4 (a) The Arrhenius plots for methanol synthesis reaction for the calculations of apparent activation energy (E_a). The points at 563 K were excluded from the fitting due to the limitation of

thermodynamic equilibrium. (b) The Arrhenius plots for RWGS for the calculations of E_a.

The apparent activation energies (E_a) for methanol synthesis and RWGS were then calculated via Arrhenius Equation ($\ln(K) = \ln(A) - E_a/RT$, where K is the reaction rate constant, A is the Arrhenius factor, R = 8.314 J mol^{-1} K^{-1}, T is the temperature). The Arrhenius plots are depicted in Fig. 4. The E_a for methanol synthesis over CZ and Pd-CZ-x (x from 0.005 to 0.04) are 59, 52, 31, 45, 62 and 70 kJ mol^{-1}, respectively. Among them, the Pd-CZ-0.01 catalyst shows the lowest E_a (31 kJ mol^{-1}), which may explain the highest methanol STY at a Pd/Cu molar ratio of 0.01. This suggests that a proper amount of Pd doping could decrease the E_a for methanol synthesis. As for the side reaction for CO formation (RWGS), the E_a over all Pd-doped samples decreased to 64-77 kJ mol^{-1} compared to the CZ catalyst (85 kJ mol^{-1}), indicating that the incorporation of Pd would also benefit the CO formation to some extent, as confirmed by Fig. 3d. The big difference in the activation energies may be explained by different chemical properties of surface Cu. Cu is promoted by Pd in the following aspects: the electronic effect, the geometric effect and the hydrogen spillover effect. The spillover affects mostly the coverages of active hydrogen atoms and thus affecting the pre-factor more than the activation energies. The electronic structure of adjacent Cu atoms would also be affected by Pd doping, probably via an electron transfer from Pd to Cu (J. Phys. Chem. **1991,** 95, 5716-5719). It is believed that the electronic effect and geometric effect would somehow influence the adsorption/desorption and activation steps, thus affecting the activation energy of a reaction. So the electronic and geometric promotion of Pd in the active sites cannot be ruled out.

We then performed a time-on-stream (TOS) test to examine the long-term stability of the Pd-CZ-0.01 catalyst. Fig. 5 shows both CO_2 conversion and methanol selectivity at 543 K for 96 h. The CO_2 conversion slightly decreases from initial 8.2% to 7.8% while the methanol selectivity increases gradually from 66% to 68% after 96 h. As a result, the final methanol STY marginally drops by only 1.7% with reference to the initial yield. After the TOS test, the Pd-CZ-0.01 catalyst was cooled down in the

H_2 atmosphere and then carefully collected for further characterizations. TEM images in Fig. S5 indicated that the "blackberry" structures were retained and the domains of Cu and PdCu lattices were still distributed on the ZnO substrates. Interestingly, we found that some of them were wrapped by few-layered overcoats with a measured layer distance of about 0.37 nm, which were believed as the amorphous ZnO as reported in the literature [41]. The migration of ZnO onto Cu surface was believed as an evidence for the strong metal-support interactions (SMSI). The growth of ZnO overcoat may protect Cu nanoparticles from reshaping and sintering caused by the structural dynamics that are found for bare copper at variable chemical potential (*Science* **2002**, 295, 2053–2055). However, whether the metastable ZnO overcoats on Cu can promote methanol synthesis is still unknown. Note that we did not observe ZnO overcoats on Cu or PdCu in all of the reduced catalyst prior to catalysis. So it seems that these ZnO overcoats form only after a prolonged time (nearly 100 h) of catalytic reaction (see Fig. S5). To better check the formation of overcoats under the reaction conditions, we have carried out additional HRTEM characterization of all used catalysts just after 8h catalytic tests. The selected TEM images are shown in Fig. S6. During the whole process of TEM imaging, we did not observe obvious amorphous ZnO overcoats on Cu or CuPd particles for all samples, unlike the case of Pd-CZ-0.01 after 96 h of TOS evaluation. This suggests that the formation of ZnO layer is undergoing a slow and ongoing process under methanol synthesis conditions. However, it should be noted that there is almost no change in catalytic activity during the TOS test (Fig. 5), which clearly reveals that ZnO overcoats do not play a decisive role in methanol synthesis. In addition, by comparing the TEM images of all used catalysts, we could not find any useful information on the influence of different Pd loading on the formation of ZnO overcoats. So there is no evidence to describe whether Pd could facilitate the formation of overcoats.

In addition, the crystal phase and chemical state of active species remained unchanged from the XRD and XPS analyses of the used Pd-CZ-0.01 catalyst (Fig.s S7 and S8).

All above analyses confirms the stability of our Pd-doped CuZn catalysts for the hydrogenation CO_2 to methanol.

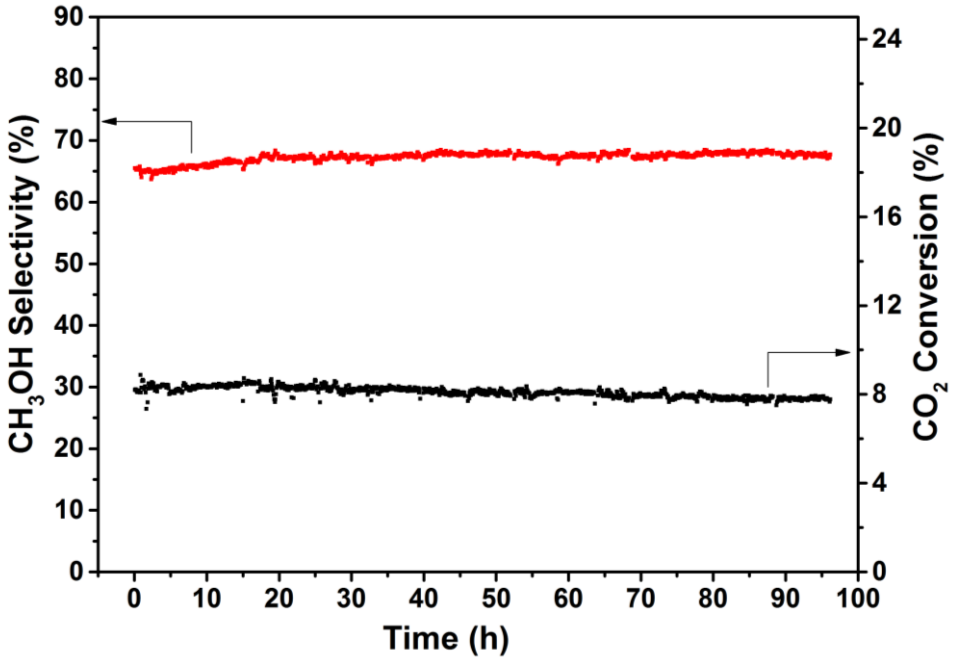

Fig. 5 Time-on-stream test of the Pd-CZ-0.01 catalyst in CO_2 hydrogenation to methanol at 543 K for 96 h. Reaction conditions: pressure=4.5 MPa, H_2/CO_2=3:1, gas flow=36 mL/min, catalyst mass=0.2 g (GHSV=10800).

3.3 Identification of active sites for methanol synthesis

It has been proposed that a hydrogen spillover mechanism is responsible for the increase in the methanol yield over Pd modified CuZn catalysts [23-26]. The dissociation of H_2 on Pd is much easier than that on Cu, which leads to a hydrogen spillover from Pd to Cu at their interfaces [44]. The transferred hydrogen species would participate in the subsequent CO_2 hydrogenation on Cu sites, thus promoting a higher methanol yield. H_2-TPD tests were then performed to confirm H_2-spillover in our Pd-CZ-x catalysts. The TPD profiles in Fig. 6 show that all samples are characteristic of a small signal at 350-600 K (Peak A) and a large H_2 desorption peak at 600-800 K (Peak B). For the CZ sample, the former peak at 451 K is assigned to the hydrogen species adsorbed on Cu in the form of Cu-H bonds [45], while the latter at 734 K stems from the heterolytically adsorbed hydrogen on the ZnO surface [46]. After the doping of Pd, the Peak A shifts positively to around 500 K, which is located

between that of CZ and the referenced Pd-ZnO sample (Fig. S9). This reveals a strong interaction at the interfaces of Pd related phase and Cu where an apparent hydrogen spillover occurs. The peak area can provide information on the amount of H_2 dissociative adsorption on Cu and Pd (metal-H bonds), thus somehow reflecting the amount of surface metal sites. Table 1 shows the calculated amount of H_2 adsorption. Apparently, the Pd-CZ-0.01 catalyst shows the largest H_2 adsorption on a catalyst weight basis (17.4 μmol g_{cat}^{-1}) as well as the largest H_2 adsorption per mole of Pd (0.32 mol mol_{Pd}^{-1}), manifesting that Pd-CZ-0.01 is more advantageous than the other Pd-doped samples in the utilization of Pd. As for the Peak B, after Pd promotion, H_2-spillover could further increase the heterolytic hydrogen stored on the ZnO surface through the Cu-ZnO interfaces, which can explain the broadening, intensification and low-temperature shift of the Peak B with the increase of Pd loading. To provide more evidence for hydrogen spillover, we have supplemented H2 TPR tests of O2 pretreated samples and the result is shown in Fig. S10. It can be clearly seen that the reduction of CuO for all the Pd doped samples is greatly facilitated as their reduction peaks shift to much lower temperatures when compared to the referenced CZ sample. The peak temperature can be brought down from 484 K for CZ to as low as 428 K even with the presence of tinny amount of Pd doping in Pd-CZ-0.005. Such shift strongly supports the idea of hydrogen spillover.

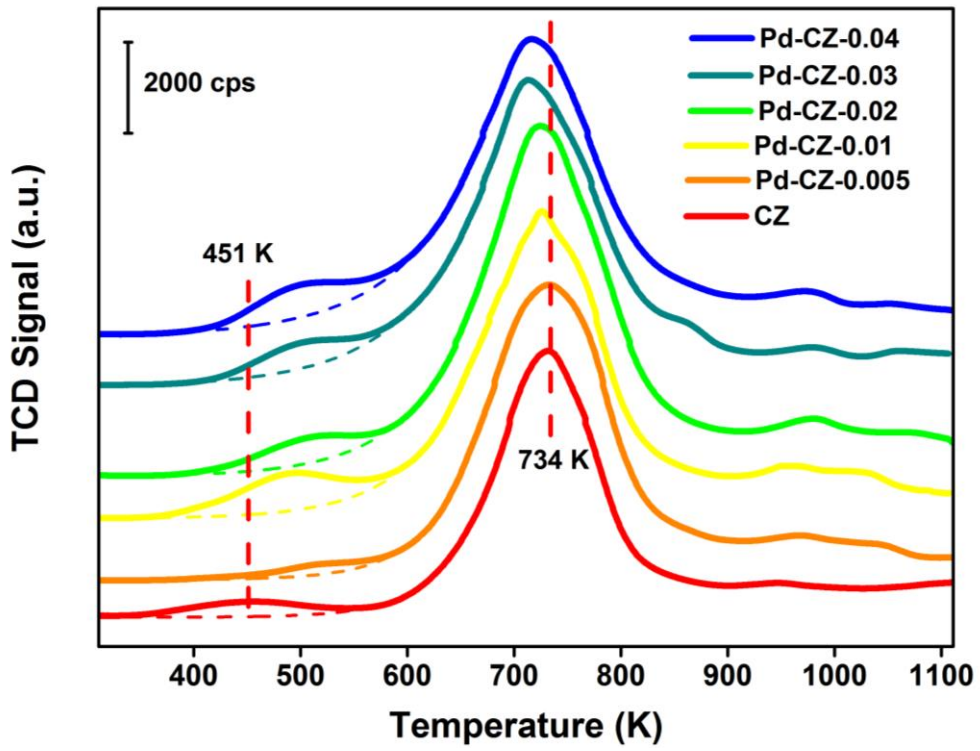

Fig. 6 H_2-TPD profiles of different catalysts with the curved dash lines representing the exponential background for the shoulder peak and the straight dash lines marking the most distinctive desorption peaks of CZ.

Table 1 H_2 desorption calculated from the peak at 350-600 K in H_2-TPD profiles.

Catalysts	peak position (K)	H_2 desorption per gram of catalyst[a] (μmol g_{cat}^{-1})	H_2 desorption per mole of Pd[a] (mol mol_{Pd}^{-1})
CZ	451	7.5	-
Pd-CZ-0.005	516	3.8	0.12
Pd-CZ-0.01	490	17.4	0.32
Pd-CZ-0.02	507	8.3	0.08
Pd-CZ-0.03	498	9.9	0.05
Pd-CZ-0.04	498	13.3	0.06

[a] H_2 desorption stands for chemisorbed hydrogen on metal species (Cu or PdCu).

Although the hydrogen spillover contributes a lot to the methanol yield, the exact nature of active sites still remains unclear. For commercial CuZn based catalysts, the

active sites for methanol synthesis are generally believed to be either CuZn alloy (*Science* **2012**, 336, 893-897) or Cu-ZnO interfaces (*Science* **2017**, 355, 1296-1299). The ZnO component is crucial to methanol synthesis and its role cannot be neglected. However, it is still very challenging to accurately quantify the above two types of active sites for commercial CuZn catalysts. Instead, the assessment of Cu surface area is normally used to correlate with the catalytic performance as the more exposed surface Cu means the more interface Cu (CuZn or Cu-ZnO). For a simplification, we would only evaluate the chemistry of Cu surface after the modification of Pd in this current work. Moreover, surface bimetallic sites such as PdCu, PdZn, CuZn have also been regarded as active sites for methanol synthesis from CO_2 hydrogenation in the literature [28]. In fact, in this work only PdCu bimetallic phase was directly determined from HRTEM analysis, but it is very difficult to quantify the surface PdCu sites. Fortunately, the chemisorption technique could provide information not only on the Cu surface areas but also on the types of Cu species.

The Cu surface area (SA) was measured by means of N_2O chemisorption, which gave the amount of Cu sites exposed to the reactants. Note that during the pre-oxidation treatment with N_2O under our conditions, only surface Cu was oxidized to Cu_2O while Pd remained in metallic phase [48], ruling out the interference by Pd. During the subsequent H_2-TPR, the surface Cu_2O was reduced to metallic Cu, resulting in the quantification of H_2 consumption as depicted in Fig. 7. The Cu SA was calculated based on the calibration plot in Fig. S11 and the results are displayed in Table 2. Apart from the case of Pd-CZ-0.02, the overall Cu SA shows a decreasing trend with the increasing Pd loading due to the blocking of surface Cu sites by Pd. As for the Pd-CZ-0.04 catalyst with the highest Pd loading, the Cu SA drops to 2.1 $m^2 g^{-1}$, which is much smaller than the undoped CZ sample (7.2 $m^2 g^{-1}$). Such a decrease in Cu SA at high coverage of Pd agrees well with earlier reported Pd modified CuZnAl catalysts [23].

Table 2 Cu surface area based on TPR peak fitting and methanol TOF at 523 K and 543 K.[a]

Catalyst	Cu_{all} SA ($m^2\ g^{-1}$) [b]	$Cu_{red.}$ SA ($m^2\ g^{-1}$) [c]	$TOF_{Methanol}$ ($\times10^{-3}\ s^{-1}$) at 523 K [d]	$TOF_{Methanol}$ ($\times10^{-3}\ s^{-1}$) at 543 K [d]
CZ	7.2	0.8	2.53	4.20
Pd-CZ-0.005	6.8	1.2	3.42	5.20
Pd-CZ-0.01	5.0	5.0	11.8	14.8
Pd-CZ-0.02	6.2	4.0	7.14	9.56
Pd-CZ-0.03	2.7	2.7	13.5	19.8
Pd-CZ-0.04	2.1	2.1	14.3	21.3

[a] Cu SA was calculated with reference to 1.46×10^{19} Cu m^{-2} [47]. [b] Cu_{all} stands for the overall surface Cu. [c] $Cu_{red.}$ stands for the surface Cu sites indicated by peak(s) at lower than 440 K. [d] Methanol TOF was calculated based on the assumption of each surface Cu atom as one active site.

We then calculated the methanol turnover frequency (TOF) based on the assumption that each surface Cu is the one site for catalytic CO_2 hydrogenation to methanol. The methanol TOF shows an increasing trend with Pd loading, suggesting that the Pd modified surface Cu sites are more active than undoped Cu sites. Importantly, the comparison between Pd-CZ-0.01 and CZ demonstrates that a minor modification with 1% Pd can increase the methanol TOF by 4.7 times from 2.53×10^{-3} to $1.18\times10^{-2}\ s^{-1}$ at 523 K and 3.5 times from 4.20×10^{-3} to $1.48\times10^{-2}\ s^{-1}$ at 543 K (Table 2). Such enhancement encouraged us to further explore the Pd modified Cu sites. Moreover, the methanol STY is not linearly correlated to the overall Cu SA (Fig. S12), suggesting that not all surface Cu atoms can offer the active sites for CO_2 hydrogenation reaction.

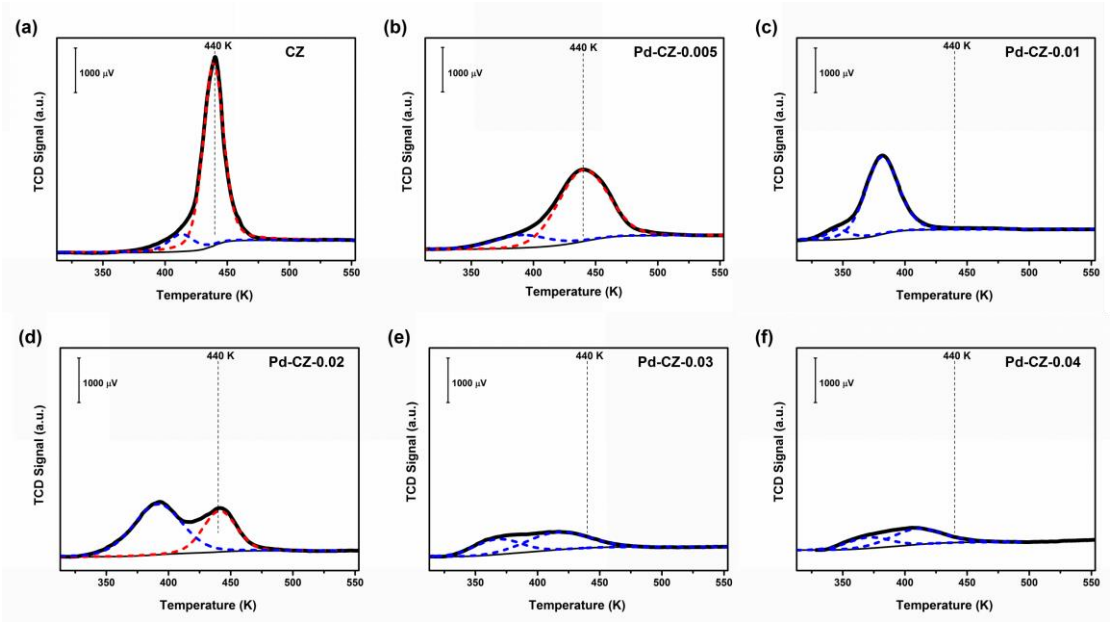

Fig. 7 Surface H_2-TPR spectra following the N_2O-oxidation treatment of CZ (a), Pd-CZ-0.005 (b), Pd-CZ-0.01 (c), Pd-CZ-0.02 (d), Pd-CZ-0.03 (e) and Pd-CZ-0.04 (f). The peak at 440 K, marked with red dashed line, arises from freestanding Cu sites. The reduction peaks at lower than 440 K, colored in blue, arise from reducible Cu sites.

Fig. 7 shows the deconvolution of TPR curves of all catalysts. The CZ sample shows a dominant reduction peak at 440 K as well as a minor peak at 412 K. The major peak can be assigned to the freestanding surface Cu upon N_2O oxidation, while the small one represents the more reducible Cu species at Cu-ZnO interfaces as it has been accepted that the coverage of ZnO can enhance the reducibility of Cu [49, 50]. After the doping of Pd, the signal of Pd-CZ-0.005 become broad due to the hydrogen spillover caused by Pd. Sykes et al. reported the hydrogen spillover effect of atomically dispersed Pd on Cu(111) surface which is distinctive even at a Pd coverage of 0.01 monolayer [44]. Interestingly, the Pd-CZ-0.01 sample exhibits a nearly singlet peak at 381 K, suggesting that the surface Cu in Pd-CZ-0.01 is evenly decorated with Pd atoms which brings spillover hydrogen to cover the overall surface Cu sites. The Pd-CZ-0.02 sample shows two distinctive reduction peaks located at 391 and 440 K. With further increasing the Pd loading the Pd-CZ-0.03 and Pd-CZ-0.04 catalysts do not show any peak at 440 K or above, suggesting that overall surface Cu domains are

affected by Pd *via* hydrogen spillover. Based on the above analyses, we divided the surface Cu sites into two main types: freestanding Cu (440 K) and reducible Cu (below 440 K, denoted as $Cu_{red.}$) caused by hydrogen spillover from Pd (Pd-CZ-x) or Cu/ZnO interfaces in the CZ sample. It should be noted that the effects of Pd, PdCu, CuZn or even Cu/ZnO interfaces on the creation of the reducible Cu are included in the $Cu_{red.}$ type. In the CO_2 hydrogenation reaction, these above phases could keep the adjacent Cu surface in a more reduced state by the spilled-over hydrogen, thus counteracting the oxidizing effect of CO_2 or H_2O.

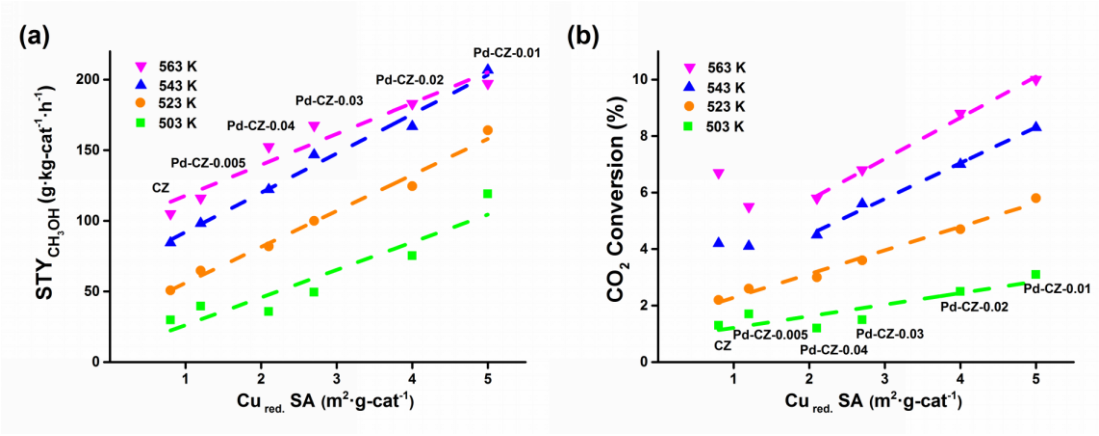

Fig. 8 Linear plots of (a) methanol STY and (b) CO_2 conversion against $Cu_{red.}$ SA. Stacked lines represent linear fitting of data points grouped by reaction temperature. In (b), the points of CZ and Pd-CZ-0.005 at 543 K and 563 K were excluded from the fitting.

The SA of $Cu_{red.}$ sites are calculated at different Pd loadings and described in Table 2. It is found that the $Cu_{red.}$ SA goes up to a maximum of 5.0 m^2 g^{-1} for the Pd-CZ-0.01 sample and then declines with a further increase of Pd loading, which resembles the volcano-shaped variation trend of methanol STY versus Pd loading. So we propose that there must be some relationship between methanol STY and $Cu_{red.}$ SA. When the methanol STY is plotted against the Cu_{red} SA, as shown in Fig. 8a, a nearly linear correlation is obtained at all reaction temperatures, indicating that the $Cu_{red.}$ sites are indeed the active sites for methanol synthesis from CO_2 hydrogenation. The Pd-CZ-0.01 catalyst has the largest SA of $Cu_{red.}$, accounting for the highest methanol STY among all tested samples. A further increase in Pd loading leads to the drop of the activity, which is probably because the effect of hydrogen spillover from Pd is not

capable of overcoming the large loss of exposed Cu surface (2.1 m^2 g^{-1} for Pd-CZ-0.04 versus 5.0 m^2 g^{-1} for Pd-CZ-0.01). So, the aforementioned volcano-shaped relationship between methanol yield and Pd loading can be explained by a balance between the hydrogen spillover effect of Pd and the reduction of surface Cu area caused by Pd blocking. At last, the CO_2 conversion was then correlated with the $Cu_{red.}$ SA, and it also shows a nearly linear relationship except for the data of CZ and Pd-CZ-0.005 at 523 and 543 K (Fig. 8b). Note that the deviation of the CZ and Pd-CZ-0.005 sample at 523 and 543 K may be explained by the additional contribution from the freestanding Cu sites activated at a high temperature for the RWGS reaction. This is further confirmed by the correlation between CO STY and $Cu_{red.}$ SA (Fig. S13).

4. Conclusions

In conclusion, we have demonstrated a facile strategy to modulate the chemistry of surface Cu sites *via* doping of Pd over the CuZn catalysts with improved activity for methanol synthesis from CO_2 hydrogenation. The Pd doping was established in a one-pot synthesis by adopting a polyol reduction method in diethylene glycol. The characterizations of XRD, TEM and HAADF-STEM confirm all the Pd-CZ-x samples show a high dispersion of Pd on Cu nanoparticles supported on ZnO. As the molar ratio of Pd to Cu is gradually increased from 0 to 0.04, we obtain a volcano-shaped relationship between methanol STY and Pd loading. The Pd-CZ-0.01 sample shows the best performance, with a methanol STY of 207 g kg_{cat}^{-1} h^{-1}, 2.5 times that of the undoped CZ catalyst, and with a TOF of 0.015 s^{-1}, 3.5 times that of CZ catalyst at 543 K. Kinetic studies shows that the Pd modification significantly reduces the E_a required for methanol synthesis from 59 kJ mol^{-1} over CZ to 31 kJ mol^{-1} over Pd-CZ-0.01. Behind the volcano-shaped relationship, we found a balance between the hydrogen spillover effect of Pd and the reduction of surface Cu area caused by Pd blocking. In addition, the chemisorption analyses reveal the strong interactions between Pd and Cu at their interfaces, where a hydrogen spillover is taken place from Pd to Cu, thus

generating more reducible Cu sites. Importantly, these reducible Cu sites are the real active sites for methanol synthesis, as confirmed by a linear correlation of the methanol STY with the reducible Cu SA. Thus, this work provides insight into the surface modification of Cu-based catalysts for more efficient methanol synthesis.

Acknowledgement

This work was supported by the National Natural Science Foundation of China (21373153, 21603244) and the Fundamental Research Funds for the Central Universities (2042016kf0180).

References

[1] W.W. Kaeding, S.A. Butter, J. Catal. 61 (1980) 155-164.

[2] G.A. Olah, A. Goeppert, G.K.S. Prakash, J. Org. Chem. 74 (2008) 487-498.

[3] G.A. Olah, Angew. Chem. Int. Ed. 44 (2005) 2636-2639.

[4] F. Liao, X.-P. Wu, J. Zheng, M.M.-J. Li, A. Kroner, Z. Zeng, X. Hong, Y. Yuan, X.-Q. Gong, S.C.E. Tsang, Green Chem. 19 (2017) 270-280.

[5] H. Herzog, B. Eliasson, O. Kaarstad, Sci. Am. 282 (2000) 72-79.

[6] K.M.K. Yu, I. Curcic, J. Gabriel, S.C.E. Tsang, ChemSusChem 1 (2008) 893-899.

[7] J.S. Lee, K.H. Lee, S.Y. Lee, Y.G. Kim, J. Catal. 144 (1993) 414-424.

[8] K. Klier, Adv. Catal. 31 (1982) 243-313.

[9] X. Liu, G. Lu, Z. Yan, J. Beltramini, Ind. Eng. Chem. Res. 42 (2003) 6518-6530.

[10] K.M. VandenBussche, G.F. Froment, J. Catal. 161 (1996) 1-10.

[11] E.L. Kunkes, F. Studt, F. Abild-Pedersen, R. Schloegl, M. Behrens, J. Catal. 328 (2015) 43-48.

[12] C. Zhong, X. Guo, D. Mao, S. Wang, G. Wu, G. Lu, RSC Adv. 5 (2015) 52958-52965.

[13] R. Ladera, F.J. Perez-Alonso, J.M. Gonzalez-Carballo, M. Ojeda, S. Rojas, J.L.G.

Fierro, Appl. Catal. B-Environ. 142 (2013) 241-248.
[14] P. Gao, F. Li, N. Zhao, F. Xiao, W. Wei, L. Zhong, Y. Sun, Appl. Catal. A-Gen. 468 (2013) 442-452.
[15] F. Arena, G. Mezzatesta, G. Zafarana, G. Trunfio, F. Frusteri, L. Spadaro, J. Catal. 300 (2013) 141-151.
[16] M. Saito, Catal. Surv. Jpn. 2 (1998) 175-184.
[17] F. Studt, M. Behrens, E.L. Kunkes, N. Thomas, S. Zander, A. Tarasov, J. Schumann, E. Frei, J.B. Varley, F. Abild-Pedersen, J.K. Norskov, R. Schloegl, Chemcatchem 7 (2015) 1105-1111.
[18] I.A. Fisher, A.T. Bell, J. Catal. 172 (1997) 222-237.
[19] V. Nguyen Thi Thuy, L. Luu Cam, T. Nguyen, C. Hoang Tien, Int. J. Nanotechnol. 12 (2015) 405-415.
[20] F. Arena, K. Barbera, G. Italiano, G. Bonura, L. Spadaro, F. Frusteri, J. Catal. 249 (2007) 185-194.
[21] X. Dong, H. Zhang, G. Lin, Y. Yuan, K.R. Tsai, Catal. Lett. 85 (2003) 237-246.
[22] B. Shen, X. Wu, H. Zhang, G. Lin, X. Dong, Acta Chim. Sin. 62 (2004) 1721-1728.
[23] I. Melian-Cabrera, M.L. Granados, J.L.G. Fierro, J. Catal. 210 (2002) 285-294.
[24] I. Melian-Cabrera, M.L. Granados, J.L.G. Fierro, J. Catal. 210 (2002) 273-284.
[25] I. Melian-Cabrera, M.L. Granados, J.L.G. Fierro, Catal. Lett. 79 (2002) 165-170.
[26] M. Sahibzada, D. Chadwick, I.S. Metcalfe, Catal. Today 29 (1996) 367-372.
[27] X. Jiang, N. Koizumi, X. Guo, C. Song, Appl. Catal. B-Environ. 170 (2015) 173-185.
[28] H. Bahruji, M. Bowker, G. Hutchings, N. Dimitratos, P. Wells, E. Gibson, W. Jones, C. Brookes, D. Morgan, G. Lalev, J. Catal. 343 (2016) 133-146.
[29] F. Bonet, V. Delmas, S. Grugeon, R.H. Urbina, P.Y. Silvert, K. Tekaia-Elhsissen, Nanostruct. Mater. 11 (1999) 1277-1284.
[30] D. Wang, C. Song, Z. Hu, X. Zhou, Mater. Lett. 59 (2005) 1760-1763.

[31] B. Wiley, T. Herricks, Y. Sun, Y. Xia, Nano Lett. 4 (2004) 1733-1739.

[32] Q. Zhang, T.R. Chou, B. Russo, S.A. Jenekhe, G. Cao, Angew. Chem. Int. Ed. 47 (2008) 2402-2406.

[33] I. Beinik, M. Hellstrom, T.N. Jensen, P. Broqvist, J.V. Lauritsen, Nat. Commun. 6 (2015) 8845-8853.

[34] P. Swift, D. Shuttleworth, M.P. Shea (Eds.), Practical Surface Analysis by Auger and X-ray Photoelectron Spectroscopy, Wiley, London, 1983, p. 477.

[35] H. Bahruji, M. Bowker, W. Jones, J. Hayward, J.R. Esquius, D.J. Morgan, G.J. Hutchings, Faraday Discuss., 197 (2017) 309-324.

[36] K.S.W. Sing, D.H. Everett, R.A.W. Haul, L. Moscou, R.A. Pierotti, J. Rouquerol, T. Siemieniewska, Pure Appl. Chem. 57 (1985) 603-619.

[37] G.H. Graaf, P. Sijtsema, E.J. Stamhuis, G.E.H. Joosten, Chem. Eng. Sci. 41 (1986) 2883-2890.

[38] T. Fujitani, M. Saito, Y. Kanai, M. Takeuchi, K. Moriya, T. Watanabe, M. Kawai, T. Kakumoto, Chem. Lett. 6 (1993) 1079-1080.

[39] T. Fujitani, M. Saito, Y. Kanai, T. Kakumoto, T. Watanabe, J. Nakamura, T. Uchijima, Catalysis Letters, 25 (1994) 271-276.

[40] G.H. Graaf, H. Scholtens, E.J. Stamhuis, A. Beenackers, Chem. Eng. Sci. 45 (1990) 773-783.

[41] T. Lunkenbein, J. Schumann, M. Behrens, R. Schloegl, M.G. Willinger, Angew. Chem. Int. Ed. 54 (2015) 4544-4548.

[42] C.T. Campbell, K.A. Daube, J.M. White, Surf. Sci. 182 (1987) 458-476.

[43] S. Kattel, P.J. Ramirez, J.G. Chen, J.A. Rodriguez, P. Liu, Science 355 (2017) 1296-1299.

[44] G. Kyriakou, M.B. Boucher, A.D. Jewell, E.A. Lewis, T.J. Lawton, A.E. Baber, H.L. Tierney, M. Flytzani-Stephanopoulos, E.C.H. Sykes, Science 335 (2012) 1209-1212.

[45] K.C. Waugh, Solid State Ion. 168 (2004) 327-342.

[46] F. Arena, G. Italiano, K. Barbera, S. Bordiga, G. Bonura, L. Spadaro, F. Frusteri, Appl. Catal. A-Gen. 350 (2008) 16-23.

[47] J.W. Evans, M.S. Wainwright, A.J. Bridgewater, D.J. Young, Appl. Catal. 7 (1983) 75-83.

[48] X. Wei, X.-F. Yang, A.-Q. Wang, L. Li, X.-Y. Liu, T. Zhang, C.-Y. Mou, J. Li, J. Phy. Chem. C 116 (2012) 6222-6232.

[49] G. Fierro, M. LoJacono, M. Inversi, P. Porta, F. Cioci, R. Lavecchia, Appl. Catal. A-Gen. 137 (1996) 327-348.

[50] R. Burch, S.E. Golunski, M.S. Spencer, J. Chem. Soc. Faraday. T. 86 (1990) 2683-2691.